Atmospheric Research 315 (2025) 107907

Contents lists available at ScienceDirect

Atmospheric Research

journal homepage: www.elsevier.com/locate/atmosres

Enhanced impact of western North Pacific tropical cyclones on El Niño intensity in the past 40 years

Xingfang Huang [a], Fei Huang [a,b,c], Hengxin Qu [a], Tingting Fan [d], Shibin Xu [a,*]

[a] Department of Marine Meteorology, Ocean University of China, Qingdao, China
[b] Frontier Science Center for Deep Ocean Multispheres and Earth System (FDOMES) and Physical Oceanography Laboratory, Ocean University of China, Qingdao, China
[c] Laoshan Laboratory, Qingdao, China
[d] Shandong Advanced Optoelectronic Materials and Technologies Engineering Laboratory, School of Mathematics and Physics, Qingdao University of Science and Technology, Qingdao, China

ARTICLE INFO

Keywords:
Tropical cyclone
El Niño
Kelvin wave
ENSO dynamics

ABSTRACT

Tropical cyclones (TCs) in the western North Pacific (WNP) can modulate the intensity of ENSO by weakening the Walker circulation and exciting or enhancing the eastward oceanic Kelvin waves. We find that WNP TCs have played an increasingly important role in the development of El Niño over the past 40 years, and that TCs contribute more to atmospheric circulation, SST and thermocline depth anomalies. The accumulated cyclone energy (ACE) in the WNP shows an enhanced explanatory capability for the Niño 3.4 index. TCs excite oceanic Kelvin waves with greater amplitudes compared to the past. Through diagnostic analysis of the temperature tendency equation, it is also found that TCs contribute more strongly to thermocline feedback and zonal advection feedback three months later. Consequently, it can be concluded that TCs play an increasingly significant positive feedback role in ENSO dynamics in the current climate context.

1. Introduction

The El Niño-Southern Oscillation (ENSO) represents the most robust interannual ocean–atmosphere coupling mode, exerting profound impacts on global weather and climate (Bjerknes, 1969; Chia and Ropelewski, 2002; Jin, 1996, 1997; Jin and An, 1999; Jin et al., 2003; Wang and Chan, 2002; Yeh et al., 2009). Tropical cyclones (TCs) are deep cyclonic vortices that generate from warm ocean surfaces, their genesis position, lifetime and intensity are significantly affected by ENSO (Chia and Ropelewski, 2002; Wang and Chan, 2002; Wang et al., 2013). The Western North Pacific (WNP) is among the most active regions globally for TC genesis, accounting for approximately 30 % of all TCs worldwide. These TCs are integral to the Earth's climate system, influencing temperature and precipitation patterns and modulating ocean circulation. During El Niño years, TC activity in the WNP typically intensifies due to enhanced cyclogenesis (Camargo and Sobel, 2005).

Recent studies, however, have increasingly identified a bidirectional relationship, wherein TCs also influence ENSO events. Observational and numerical experiments have demonstrated that TCs affect ENSO evolution (Li et al., 2023; Lian et al., 2019; Sriver et al., 2013; Wang and Li, 2022a, 2022b; Wang et al., 2019; Wang and Tan, 2023). Research has shown that high-frequency wind stress can trigger or boost El Niño events. Intraseasonal oscillations in the Indian Ocean generate eastward Kelvin waves, affecting sea surface temperature and enhancing El Niño (McPhaden and Yu, 1999). Similarly, West Wind Bursts (WWBs) can intensify El Niño through ocean-atmosphere interactions (Fedorov, 2002; Fedorov et al., 2015). These interactions can shift the tropical Pacific from a neutral to an El Niño state. A strong link exists between frequent westerly wind stress and El Niño occurrences near the equator. Improving the representation of WWBs in forecast models will greatly improve ENSO prediction capabilities (Lopez and Kirtman, 2014).

TCs are associated with approximately 69 % of WWBs, displaying a remarkably similar wind field structure (Harrison and Giese, 1991; Lian et al., 2018; Lian et al., 2019; Liang and Fedorov, 2021). Such winds contribute to the warming of SST in the tropical Pacific (Fedorov et al., 2010), and the effects of TCs on oceanic and atmospheric conditions can persist for extended periods (Hart et al., 2007). Consequently, TCs significantly influence El Niño intensity by generating westerly winds near the equator, directly affecting El Niño's development. This relationship has led to the development of an empirical ENSO forecast model based on WNP Accumulated Cyclone Energy (ACE; Wang et al., 2019). Additionally, WNP TCs have been shown to influence the

* Corresponding author.
E-mail address: xushibin@ouc.edu.cn (S. Xu).

https://doi.org/10.1016/j.atmosres.2024.107907
Received 12 September 2024; Received in revised form 28 December 2024; Accepted 31 December 2024
Available online 2 January 2025

diversity of El Niño events through coupled atmospheric and oceanic linkages (Wang and Li, 2022a, 2022b).

In the context of a warming climate, the intensity, frequency, and translation speed of TCs have changed significantly. Similarly, the frequency, amplitude, diversity, and contribution of external forcings to El Niño events have also evolved (Cai et al., 2014; Elsner, 2020; Gan et al., 2023; Kang and Elsner, 2015, 2016; Yamaguchi et al., 2020; Yang et al., 2018; Yeh et al., 2009). However, it remains uncertain how the modulation of TCs on El Niño intensity may change in a warming climate. This study investigates changes in the explained variance between WNP ACE and N3.4 SST anomalies over the past 40 years. Results reveal a significant increase in the explained variance, with enhanced circulation anomalies and thermocline depth variations linked to WNP TCs. Notably, eastward-propagating downwelling oceanic Kelvin waves associated with TCs have become more prominent. The corresponding thermocline feedback and zonal advection feedback terms, which lag TCs by three months, show significant interdecadal enhancement.

2. Data and methods

2.1. Accumulated cyclone energy and TC days

The accumulated cyclone energy (ACE) used in this study is defined by Bell et al. (2000):

$$ACE = \sum_n v_n^2 \tag{1}$$

In Eq. (1) n is the n^{th} TC in each 2° × 2° latitude and longitude grid cell in TC key region, and v_n^2 is the square of the maximum sustained wind speed over 6 h. The TC key region is defined as 5°–20°N, 135°–170°E, which is the spatial range of ACE calculated in this paper. 6-hourly maximum sustained wind speed and TCs best-track dataset are obtained from the International Best Track Archive for Climate Stewardship [IBTrACS, (Knapp et al., 2010)]. TC wind is obtained from hourly reanalysis of wind field data [ERA5 (Hersbach et al., 2020), NCEP-NCAR (Kalnay et al., 1996) and NCEP-DOE (Kanamitsu et al., 2002)]. The TC days is defined as the date of TCs in the key region, and TC genesis (t_0) is the time when each TC was first recorded in TC key region, t_{-1} is 10 days before the TC genesis, and t_{+1} is 10 days after the TC genesis.

2.2. El Niño intensity and developing years

The El Niño intensity index used in this study is Niño3.4 index (N3.4) by NOAA. An El Niño event is defined as the 5 consecutive running 3-month mean of N3.4 above +0.5 °C. A moderate or above intensity El Niño event with N3.4 above +1.0 °C was selected. The definition of El Niño developing year is a year in which the equatorial Pacific develops from a neutral or La Niña state to an El Niño state, and an El Niño decaying year is defined as a year in which the El Niño changes from strong to weak. Based on the above conditions, this study selected 9 El Niño events of moderate or above intensity during 1981–2023 (1982–1983, 1986–1987, 1991–1992, 1994–1995, 1997–1998, 2002–2003, 2009–2010, 2015–2016 and 2023–2024) and we mainly focus on 9 developing years (1982, 1986, 1991, 1994, 1997, 2002, 2009, 2015 and 2023). The past 40 years were divided into two periods, P1 (1981–2000) and P2 (2001−2023). In addition, the oceanic niño index (ONI) is used in the supporting document. Monthly ONI index is available from NOAA. This study used the regression and composite of ERA5 monthly zonal and meridional wind to analyze the circulation anomaly contributed by TCs in El Niño development years and TC wind is obtained from hourly zonal and meridional wind.

2.3. Circulation index and intraseasonal oscillation index

The circulation index was calculated in this study to quantify circulation anomalies caused by TCs. The zonal and meridional circulation indices are defined as follows:

$$I_x = -(U_{200} - U_{850}) \tag{2}$$

$$I_y = -(V_{200} - V_{850}) \tag{3}$$

In Eqs. (2) and (3), zonal circulation index I_x is calculated by zonal wind at 200 hPa and 850 hPa (U_{200} and U_{850}) in 15°N − 10°S, 130°E−140°W, and the meridional circulation index I_y is calculated by meridional wind at 200 hPa and 850 hPa (V_{200} and V_{850}) in 10°N − 10°S, 130°E−170°E. The calculation regions of the meridional and zonal circulation indices are selected from the regions of the wind fields that pass the Student's t-test with a significance level of 0.05.

The Madden-Julian Oscillation (MJO) represents the intraseasonal oscillation of the tropical atmosphere. To remove its influence, the MJO index is used. During the boreal summer, intraseasonal variations exhibit a more complex spatio-temporal structure compared to the MJO. To account for these, the Boreal Summer Intraseasonal Oscillation (BSISO) index is utilized to remove the impact of intraseasonal oscillations (ISO) in summer. The MJO and BSISO indices are provided by the International Pacific Research Center (IPRC). These indices are derived by projecting band-pass filtered outgoing longwave radiation (OLR) data onto daily spatial empirical orthogonal function (EOF) patterns. Specifically, the MJO index uses 30–96 days band-pass filtering for the D-J-F period, while the BSISO index applies 10–90 days band-pass filtering for the J-J-A period, both over the 15°S-15°N latitude range. MJO or BSISO index $I_{\text{M or B}}$ can be calculated from the first two principal components (PC1 and PC2) of the EOF in Eq. (4):

$$I_{\text{M or B}} = \sqrt{PC1^2 + PC2^2} \tag{4}$$

2.4. TC in El Niño dynamics and ocean reanalysis data

In this study, linear regression was used to obtain the explained percentage, the linearly dependent component, and the linearly independent component, using binary regression of standardized variable x^*, y^* on z^* we obtain the linearly independent part of z^*:

$$\widehat{z}^*_{x,y} = \beta_1 x^* + \beta_2 y^* \tag{5}$$

In Eq. (5), $\widehat{z}^*_{x,y}$ is the part of z^* that is linearly dependent on x^*, y^*. $z^* - \widehat{z}^*_{x,y}$ is the residual or linearly independent component of z^*. $\beta_1$and β_2 are regression coefficients. Explained percentage $P_{x,y}$, P_x and P_y are calculated in Eq. (6–8):

$$P_{x,y} = \frac{\widehat{z}^*_{x,y}}{z^*} \times 100\% \tag{6}$$

$$P_x = \frac{\beta_1 x^*}{z^*} \times 100\% \tag{7}$$

$$P_y = \frac{\beta_2 y^*}{z^*} \times 100\% \tag{8}$$

The thermocline depth and heat budget analysis of the ocean were calculated using 5-day ocean reanalysis data from Simple Ocean Data Assimilation (SODA), including variables such as meridional, zonal and vertical ocean currents and seawater potential temperature. The spatiotemporal coordinates of the oceanic Kelvin wave are defined as the coordinates where the depth anomalies of thermocline, after being filtered by a 20–90 days bandpass filter, exceeds the 90th percentile.

3. Results

3.1. Enhanced explained percentage of TCs

During El Niño developing years, positive ACE anomalies are

observed in the southeast quadrant of the WNP. This study focuses on the key region of WNP ACE (5°–20°N, 135°–170°E) (Fig. S1), which corresponds to the region of positive ACE anomalies during these years. The WNP ACE leading the N3.4 index by three months demonstrates the most significant lead-lag correlation between TCs and El Niño intensity in the tropical Pacific. Previous studies reported that WNP J-A-S ACE explained approximately 51 % of O-N-D N3.4 variations from 1970 to 2016 (Wang et al., 2019).

Our calculations show a significant increase in the explained percentage of N3.4 by WNP ACE over the past 40 years (Figs. 1a and S4). Specifically, the percentage of explanation for O-N-D N3.4 by J-A-S ACE exhibits the fastest growth, at approximately +11.2 % per decade (Fig. 1a). Similar results are obtained when using the ONI index (Fig. S2). Even in ACE+N3.4 binary regression analyses, the explanatory power of J-A-S ACE for N3.4 lagged by three months is steadily increasing. While the lead-lag relationship between WNP ACE and N3.4 remains unchanged, the correlation coefficient has increased over time (Fig. 1b). After removing intraseasonal variability, the trend remains consistent (Fig. S3a), further emphasizing the growing role of TCs in ENSO forecasting systems. Even after accounting for simultaneous N3.4 influences, J-A-S ACE retains significant explanatory power with an upward trend (Fig. 1a), underscoring the importance of TCs in ENSO dynamics. Consequently, empirical forecasting models based on the correlation between J-A-S ACE and O-N-D N3.4 are expected to demonstrate enhanced forecasting skill.

Over the past 40 years, both standardized N3.4 and WNP ACE have exhibited increasing trends during El Niño events, though the growth rate of ACE exceeds that of N3.4 (Fig. 1c). After removing the mutual influences between J-A-S ACE and O-N-D N3.4, contrasting trends become evident (Fig. 1d). The linearly independent component of J-A-S ACE increases, while the independent component of O-N-D N3.4 decreases. This indicates that the faster growth of ACE during El Niño developing years explains the increased percentage of N3.4 variability attributed to WNP ACE. In a warming climate, TCs generated during El Niño events have become more intense, even though ACE does not show a significant increase across all years (including La Niña and neutral phases). Favorable conditions during El Niño years continue to drive the growth of ACE, even after removing ENSO-related trends (Fig. 1d). The consistency of results after removing intraseasonal signals indicates that such signals have minimal impact on TCs and ENSO dynamics (Fig. S3).

3.2. Enhanced impact of TCs on El Niño by atmospheric bridges

TCs modulate El Niño intensity through oceanic and atmospheric bridges (Wang et al., 2019; Wang and Tan, 2023). The TC wind field, derived from hourly reanalysis 10-m wind data, reveals strong westerly anomalies south of the key region, extending to the equator (Fig. 2a and b). The relationship between TCs and WWBs is well-documented (Lian et al., 2018), with westerly winds on the southern flank of TCs significantly affecting equatorial regions for extended periods (Hart et al., 2007). Recently, TCs have generated more pronounced westerly anomalies near the equator (Fig. 2c), corresponding to the increasing trend of ACE during El Niño developing years from P1 to P2. Different reanalysis data show almost the same TC wind (Fig. 2d–2i). More intense storms now exert stronger equatorial wind stress (Fig. S5).

At 850 hPa, large-scale westerly wind anomalies are observed south of the TC key region, driven by low-pressure systems through semi-geostrophic adjustment (Fig. 3a and b). Similarly, at 200 hPa, easterly wind anomalies are generated due to increased geopotential height caused by TC-induced convection (Fig. 3d and e). Persistent low-level westerly winds near the equator are generated by low-latitude TCs, while upper-level convection raises geopotential height and induces

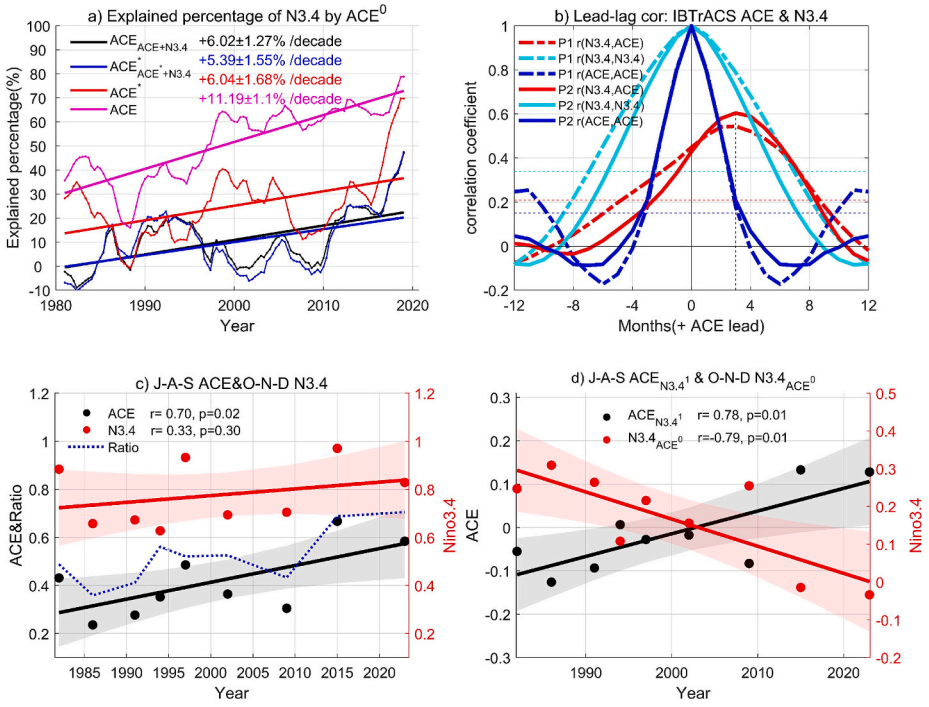

Fig. 1. (a) Explained percentage of leading ACE for O-N-D N3.4. The black and blue solid (dash-dot) lines represent the explained percentage for the leading ACE in the binary regression. The red and magenta solid (dash-dot) lines represent the explained percentage for the leading ACE in the simple regression. The text in the corresponding colors represents the growth rate and 95 % confidence interval. ACE* represents ACE after removing simultaneous N3.4. (b) The lead-lag correlation and autocorrelation of ACE and N3.4 in P1 (1981–2000) and P2 (2001–2023). The thin dashed lines of corresponding colors represent the correlation coefficients of Student's *t*-test at a 95 % confidence level calculated using effective degrees of freedom. (c) Scatterplot of the standardized time series of WNP J-A-S ACE. The black and red solid lines represent the linear fits of ACE and N3.4, and the black and red shading represents confidence interval of 95 % in regression. (d) Similar to (c), but after removing lead-lag signals. $ACE^{1}_{N3.4}$ represents ACE with 3-month lag N3.4 influence removed, and $N3.4^{0}_{ACE}$ represents N3.4 with 3-month lead ACE influence removed. (For interpretation of the references to colour in this figure legend, the reader is referred to the web version of this article.)

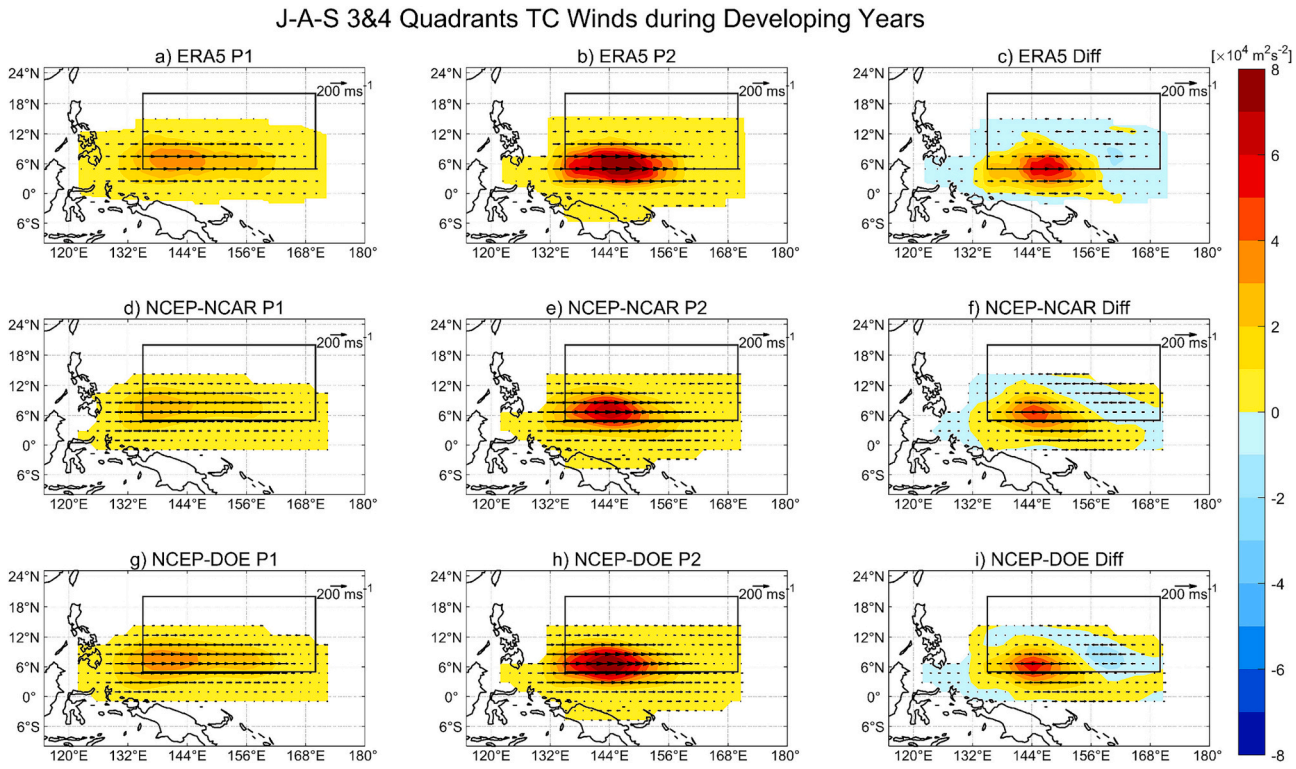

Fig. 2. Annual average accumulated zonal TC wind in TC's third and fourth quadrants in P1 (1981–2000) (a) and P2 (2001–2023) (b) base on ERA5 reanalysis. 10-m wind anomalies (vectors) and zonal wind energy (shading) are represented in this figure. Black rectangles represent the calculated regions for TCs. (c) Similar to (a) and (b) but for the difference between P1 and P2. (d)-(f), (g)-(i) are same to (a)-(c), but for NCEP/NCAR reanalysis and NCEP/DOE reanalysis II.

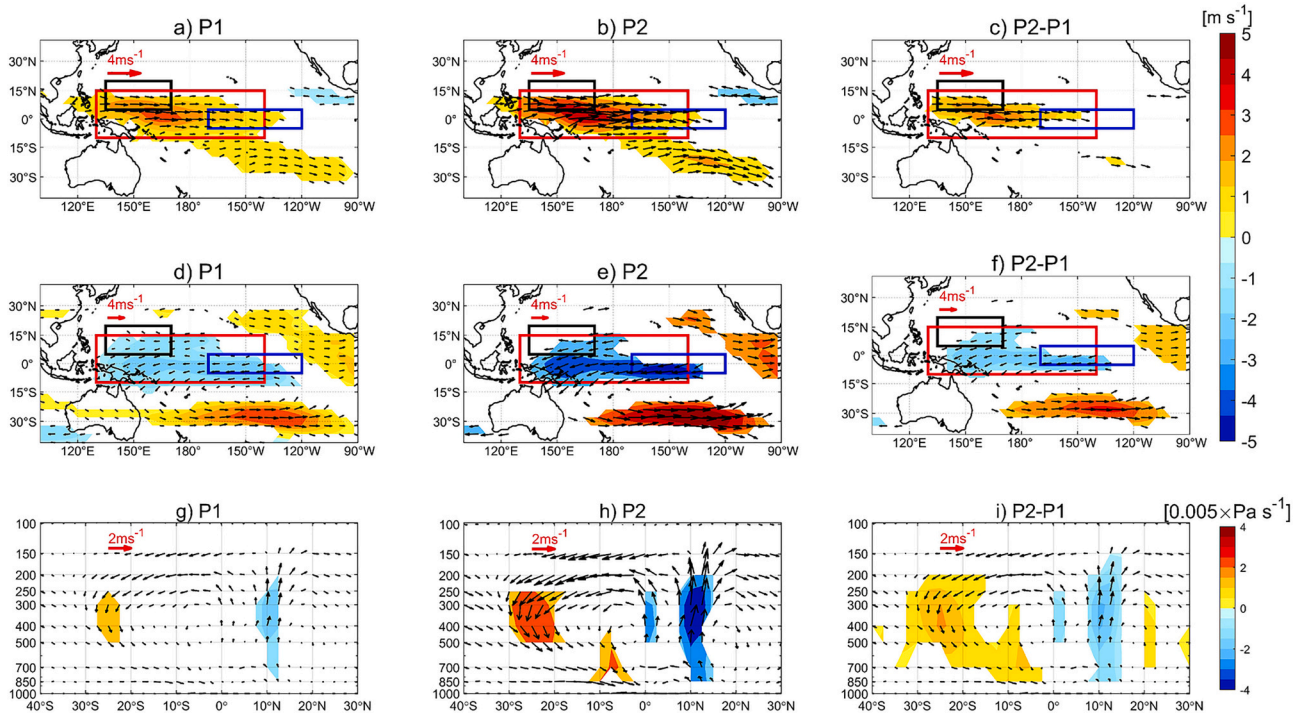

Fig. 3. (a)–(c) Composite of wind anomalies (vectors) and zonal wind anomalies (shading) at 850 hPa associated with WNP J-A-S ACE during El Niño developing years. Only zonal wind anomalies passing the $\alpha = 0.05$ Student's *t*-test are shown in the figure. Black, red and blue rectangles represent the calculated regions for ACE, circulation index and N3.4, respectively. (d)–(e) Similar to (a)–(c), but at 200 hPa. (g)–(i) Similar to (a)–(c), but at vertical–meridional plane, and the magnitude of the vertical *p*-velocity (shading) has been multiplied by −200. Only vertical *p*-velocity passing the $\alpha = 0.05$ Student's t-test are shown in the figure. Here P1 represents 1981 to 2000, and P2 represents 2001 to 2023. (For interpretation of the references to colour in this figure legend, the reader is referred to the web version of this article.)

easterly anomalies, forming an inverse Walker circulation. This inverse circulation further amplifies El Niño intensity, demonstrating the mechanism by which TCs influence ENSO via atmospheric bridges.

Comparing wind field anomalies between P1 and P2 reveals significantly stronger meridional and zonal circulations associated with ACE during P2 (Fig. 3c, f, and i). The corresponding circulation index shows a linear increase of approximately $+1.1$ m•s^{-1} per decade (Fig. S7). Stronger westerly (easterly) anomalies at 850 hPa (200 hPa), along with intensified convection, further weaken the Walker circulation, amplifying El Niño events. Correlation coefficients between the J-A-S meridional and zonal circulation indices and J-A-S ACE are approximately 0.96, indicating a robust link between TCs and simultaneous wind anomalies. These conclusions remain consistent after removing intraseasonal variability (Fig. S6).

3.3. Enhanced impact of TCs on El Niño by oceanic bridges

Another mechanism through which TCs modulate El Niño intensity is the oceanic bridge. Unlike the atmospheric bridge, the oceanic bridge operates by deepening (in the eastern Pacific) and shallowing (in the western Pacific) the thermocline through eastward-propagating downwelling oceanic Kelvin waves excited or enhanced by TCs. Thermocline fluctuation signals before and after TC genesis were calculated and are presented in Fig. 4. Ten days prior to TC genesis, thermocline depth anomalies were negligible. However, post-genesis, the thermocline in the key region became shallower, while a deepening signal appeared to the east. This deepening signal propagates eastward as a Kelvin wave, reaching the eastern equatorial Pacific within approximately two to three months (Fig. 5). These observations strongly support the role of atmospheric stochastic wind stress forcing in shaping ocean thermal structures.

These powerful storms reinforce a distinctive zonal dipole pattern of seawater potential temperature anomalies (Fig. 6a and b), highlighting their contribution to the accumulation of ocean heat content in the equatorial eastern Pacific. TCs induce a shallower thermocline in the western Pacific and a deeper thermocline in the eastern Pacific (Figs. 4 and 6d). This pattern not only underscores the pivotal role of TCs in reshaping the oceanic thermal structure but also offers valuable insights into the intricate atmosphere-ocean interactions. WNP ACE leads N3.4 by approximately three months, with the eastward Kelvin wave propagating at a velocity of ~2 m·s^{-1}, delivering the warm signal to the eastern equatorial Pacific within 2–3 months (Figs. 4 and 5). These findings suggest that TCs during the TC season exert a more significant impact on ENSO intensity than previously anticipated. Over the past 40 years, associated thermocline depth and potential temperature anomalies from WNP TCs have intensified, contributing to a more pronounced zonal thermal structure and a greater influence on El Niño intensity (Fig. 6c and d). Furthermore, intraseasonal signals were found to have minimal impact on these results (Fig. S8). Recent studies have suggested that the contribution of external forcing to ENSO SST anomalies has increased significantly since 1980, surpassing internal variability (Gan et al., 2023). This finding aligns with the observed increased contribution of TCs to El Niño.

Over the past 40 years, WNP TC ACE during El Niño developing years has shown a marked increase, with active TCs generating stronger westerly anomalies near the equator (Fig. 2c). The correspondence

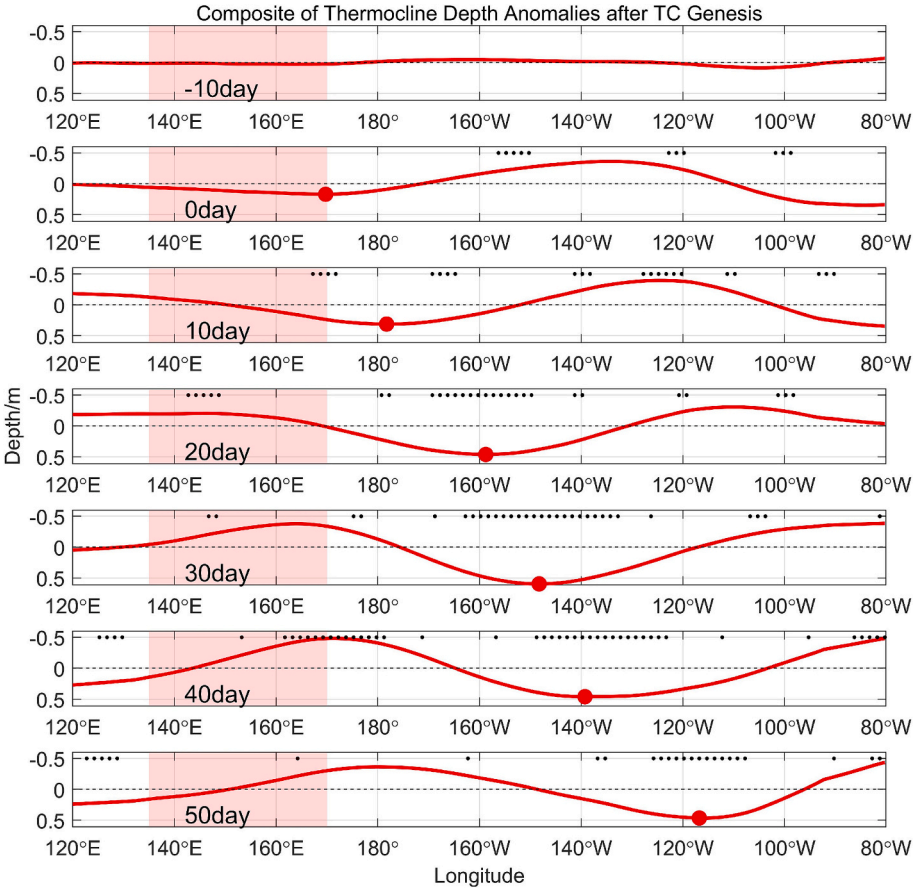

Fig. 4. Composite of thermocline depth anomalies after each TC genesis in key region from 1981 to 2023. The red solid lines represent the thermocline depth anomalies at depth–zonal plane between 5°S − 5°N. The red shading and solid circle represent TC key region and trough. 0 day is defined as the date when each TC was first recorded. Black spots denote anomalies passing the $\alpha = 0.05$ Student's *t*-test. (For interpretation of the references to colour in this figure legend, the reader is referred to the web version of this article.)

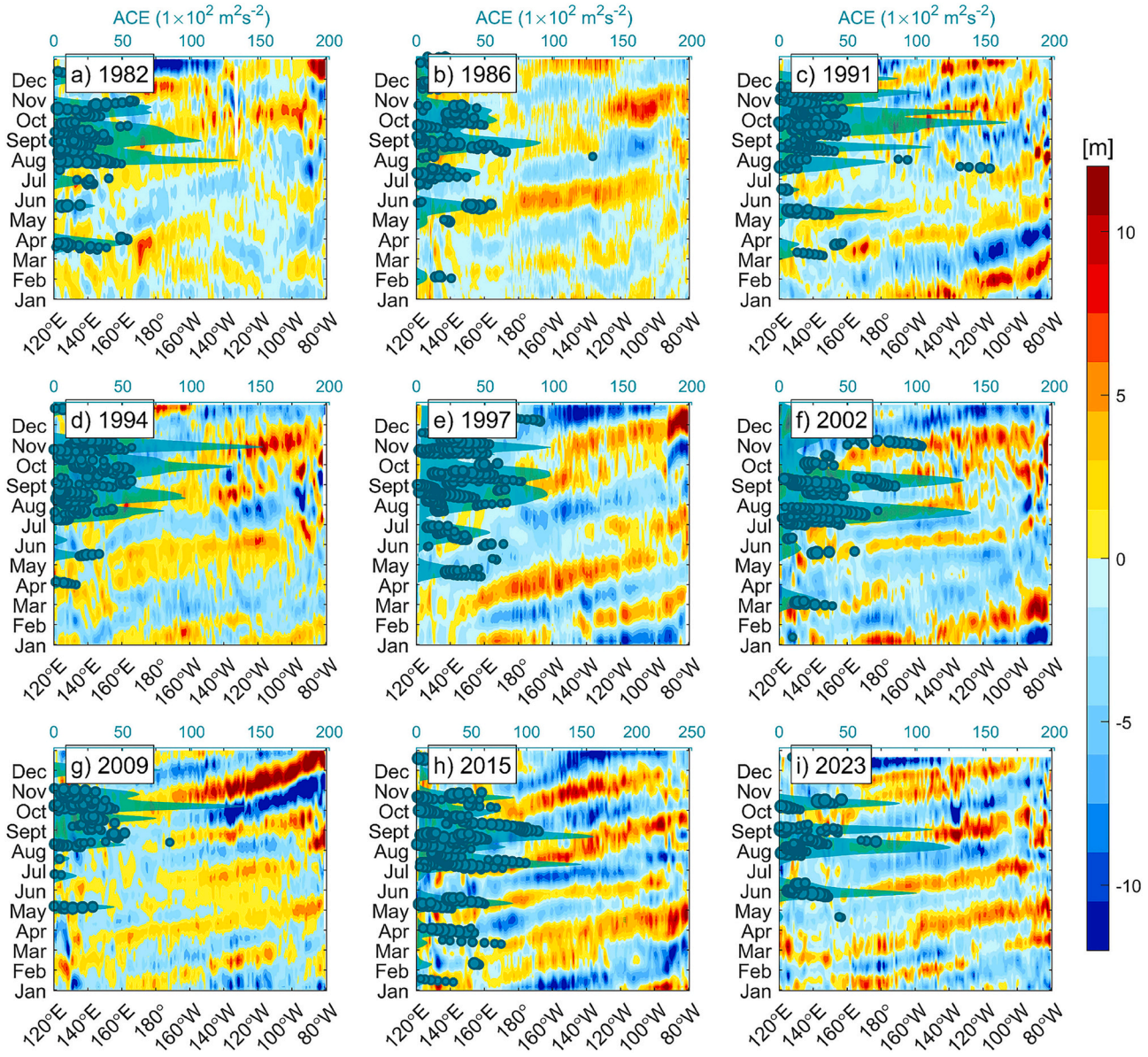

Fig. 5. (a)–(i) Hovmöller diagram of thermocline depth anomalies between 5°S − 5°N during developing years. The depth of the thermocline is calculated as the depth of the isothermal depth of 20 °C and filtered by a bandpass filter for 20–90 days. The green circles represent TC days and their corresponding longitudes. The green shade indicates the intraseasonal variation of WNP ACE. Intraseasonal signal has been removed. (For interpretation of the references to colour in this figure legend, the reader is referred to the web version of this article.)

between TC activity and eastward Kelvin waves has become increasingly evident, as shown by the Hovmöller diagram of thermocline depth anomalies (Fig. 5). TCs are frequently accompanied by eastward-propagating deepening thermocline signals (Fig. 7e), and this relationship has grown stronger over time. We analyzed equatorial thermocline depth anomalies before and after each TC genesis and examined the relationship between annual TC days and Kelvin wave activity days. Composite analyses reveal that significant eastward-propagating downwelling waves are generated after TCs (Fig. 4). Moreover, the impact of TC-induced wind fields on the thermocline has intensified, with storms producing waves of greater amplitude, thereby regulating El Niño more effectively (Fig. 7c and d).

In order to further study the contribution of TCs to El Niño dynamics and oceanic heat budget, we refer to Jin et al. (2003) and Li et al. (2023), and use the temperature tendency equation as follows:

$$\frac{\partial T'}{\partial t} = -u'\frac{\partial \overline{T}}{\partial x} - v'\frac{\partial \overline{T}}{\partial y} - \omega'\frac{\partial \overline{T}}{\partial z} - \overline{u}\frac{\partial T'}{\partial x} - \overline{v}\frac{\partial T'}{\partial y} - \overline{\omega}\frac{\partial T'}{\partial z} - u'\frac{\partial T'}{\partial x} - v'\frac{\partial T'}{\partial y} - \omega'\frac{\partial T'}{\partial z} + R \tag{9}$$

TCs can activate and enhance the eastward downwelling Kelvin waves and also cause widespread westerly winds near the equator, so we focus on the thermocline feedback term ($-\overline{\omega}\frac{\partial T'}{\partial z}$) and the zonal advection feedback term ($-u'\frac{\partial \overline{T}}{\partial x}$) of Eq. (9) (Jin, 1997; Jin and An, 1999; Li et al., 2023), as they are the primary mechanisms by which TCs modulate El Niño intensity. Since WNP ACE leads N3.4 by approximately months, we calculated the thermocline anomalies caused by TCs 3 months later. The composite evolution of thermocline depth anomalies associated with ACE is presented in Fig. 8a and b. The results demonstrate that TCs significantly contribute to the deepening (in the eastern Pacific) and shallowing (in the western Pacific) of the thermocline three months post-TC genesis during both analyzed periods. Furthermore, the amplitude of thermocline depth anomalies associated with ACE has increased

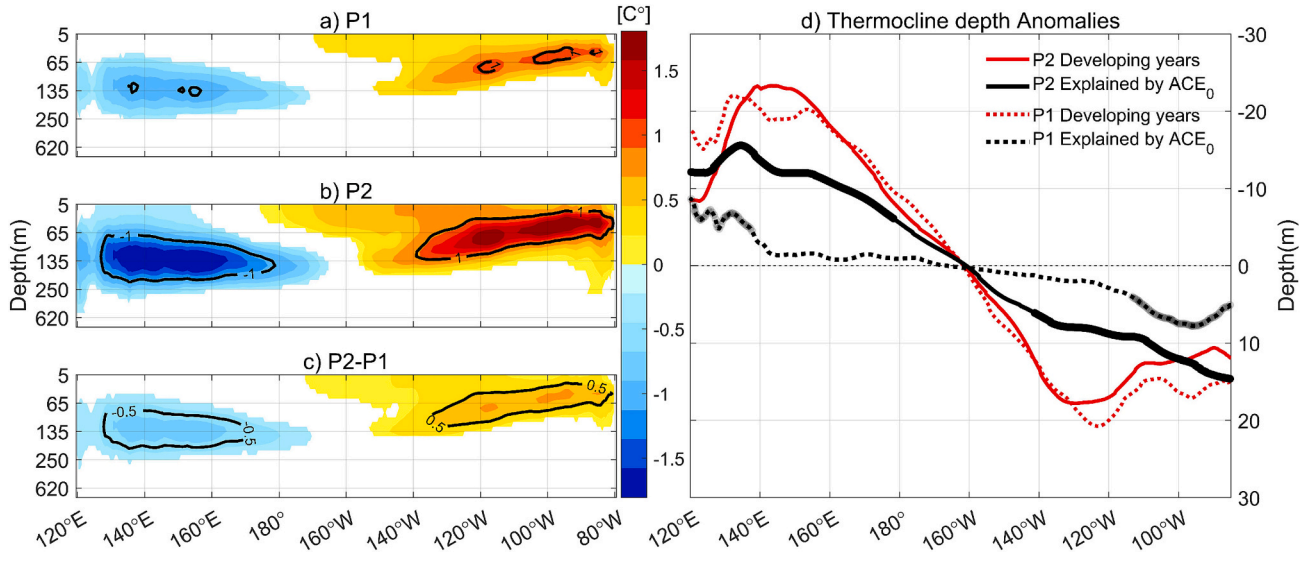

Fig. 6. (a)–(c) Composite of O-N-D potential temperature anomalies associated with ACE_0 at depth–zonal plane between 5°S − 5°N during El Niño developing years. Black contours represent the absolute value of anomalies greater than 1.0 or 0.5 °C. Only potential temperature anomalies passing the $\alpha = 0.05$ Student's *t*-test are shown in the figure. (d) Composite of O-N-D thermocline depth anomalies between 5°S − 5°N during El Niño developing years. The depth of the thermocline is calculated as the depth of the isothermal depth of 20 °C. The red solid and dashed lines represent the composite of depth anomalies in the two periods during El Niño developing years. Black is similar to red, but indicates the portion explained by ACE_0. Thicker lines pass the $\alpha = 0.05$ Student's *t*-test. ACE_0 represents leading WNP ACE. Here P1 represents 1981 to 2000, and P2 represents 2001 to 2023. (For interpretation of the references to colour in this figure legend, the reader is referred to the web version of this article.)

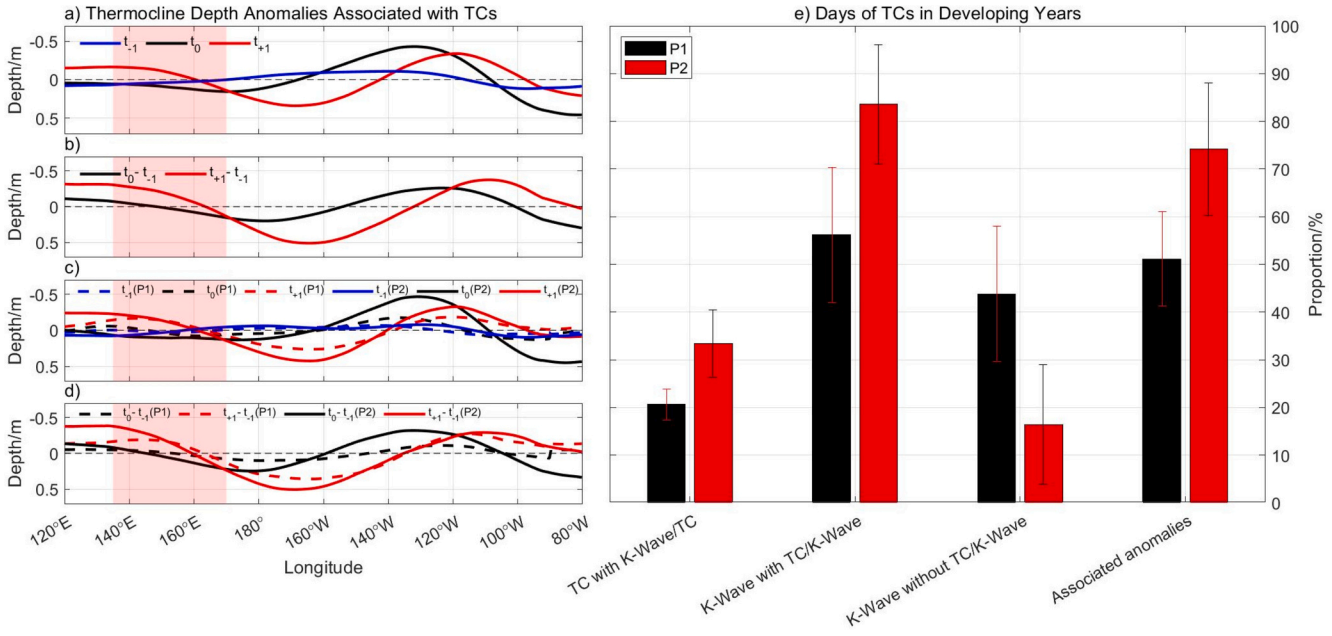

Fig. 7. (a)–(d) Composite of thermocline depth anomalies after and before TC genesis in developing years. The red (blue and black) solid lines represent the thermocline depth anomalies at depth–zonal plane between 5°S − 5°N during El Niño developing years after (before and when) TC genesis. The red shading represents TC key region. And t_0 (t_{-1} and t_{+1}) is defined as the date (10 days ago and later) when each TC was first recorded. (e) TC and Kelvin wave days in developing years of P1 (1981–2000) and P2 (2001–2023). The black and red bars (error bar) represent the (standard deviation of) percentage of days in P1 and P2, respectively. Where A/B denotes percentage of the number of days when A occurs to the number of days when B occurs. Associated anomalies denote the percentage of the anomalies associated with TCs in total anomalies. (For interpretation of the references to colour in this figure legend, the reader is referred to the web version of this article.)

during the P2 period, indicating that the oceanic impacts of TCs have become more pronounced.

The impacts of atmospheric random westerly stress forcings and their induced oceanic waves in the climate system are remarkable. These forcings contribute to positive SST anomalies, which in turn have significant implications for the intensity and frequency of TCs. In recent years, the intensity of TCs has increased significantly, a phenomenon that has been observed globally and is consistent with the projected impacts of climate change. This rise in TC intensity is evident during El Niño developing years (Fig. 1c and d). During El Niño developing years, the warming of the equatorial eastern Pacific Ocean leads to changes in atmospheric circulation, including enhanced westerly wind bursts. TCs

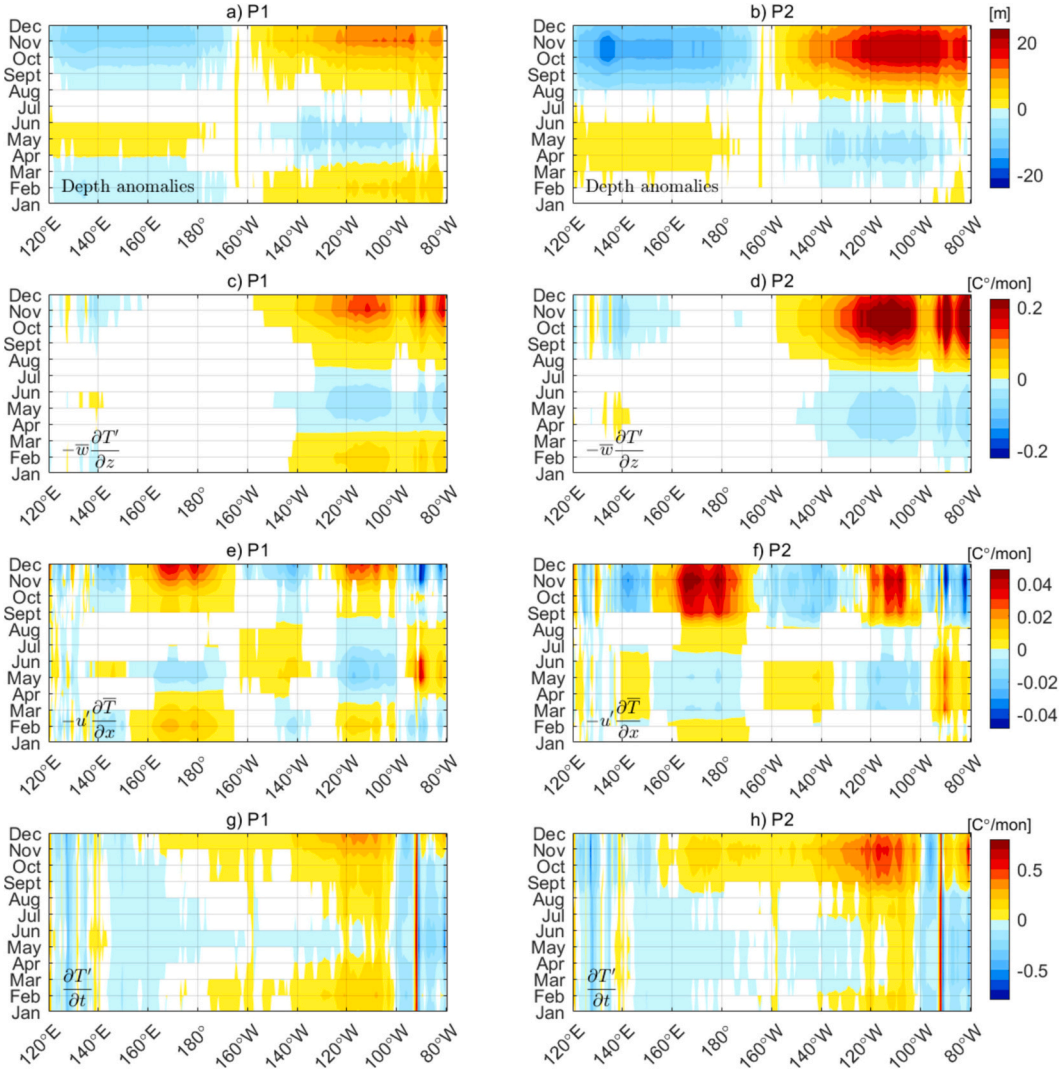

Fig. 8. (a), (b) Composite of Hovmöller diagram of thermocline depth anomalies associated with leading WNP ACE between 5°S − 5°N during P1 and P2. The depth of the thermocline is calculated as the depth of the isothermal depth of 20 °C. (c), (d) Composite of Hovmöller diagram of thermocline feedback term ($-\overline{w}\frac{\partial T'}{\partial z}$) contributed by leading WNP ACE between 5°S − 5°N during P1 and P2. (e), (f) Similar to (c), (d), but for zonal advection feedback term ($-u'\frac{\partial \overline{T}}{\partial x}$). (g), (h) Similar to (c), (d), but for total temperature tendency ($\frac{\partial T'}{\partial t}$). Only anomalies passing the $\alpha = 0.05$ Student's *t*-test are shown in the figure. Here P1 represents 1981 to 2000, and P2 represents 2001 to 2023. Intraseasonal signal has been removed.

provide positive feedback to ENSO development by enhancing ACE during El Niño years, which further amplifies El Niño intensity. Neglecting the influence of TCs could significantly reduce the accuracy of ENSO forecasting systems (Li et al., 2023; Lian et al., 2019; Wang et al., 2019).

This positive feedback mechanism has strengthened in recent years, highlighting the increasing significance of TC-related thermocline and zonal advection feedbacks (Figs. 8c–8h). These feedback terms show no significant changes in ENSO development between the two periods analyzed (Fig. S9), except for the components directly linked to ACE (Fig. 8). Among these, vertical convection of temperature anomalies stands out as the dominant factor. This process leads to subsurface warming in the eastern Pacific, which contributes to El Niño SST anomalies under the influence of the average vertical ocean current (Fig. 8c and d). The evolution of thermocline feedback closely mirrors the evolution of thermocline depth anomalies (Figs. 8a–8d), both peaking during O-N-D and lagging the TC season by approximately three months. Zonal advection feedback also shows an increasing trend, although its magnitude is lower than that of thermocline feedback. Its evolution pattern differs from thermocline feedback (Fig. 8e and f). TCs generate advection feedback that contributes to warming in the central and eastern equatorial Pacific, consistent with results from numerical experiments (Li et al., 2023).

4. Conclusions and disscussion

Numerous studies have shown that TCs enhance the intensity of El Niño, but how this effect may evolve under changing climate conditions remains unclear. In this study, we examined the contribution of TCs to El Niño intensity over the past 40 years. Our results indicate that TCs play an increasingly important role in providing positive feedback to El Niño development. During El Niño developing years, favorable cyclonic conditions strengthen WNP ACE, which subsequently amplifies N3.4 three months later. This feedback arises from coupled atmosphere-ocean processes.

Low-latitude TC activity is now producing longer-lasting and stronger westerly winds near the equator. The relationship between TCs and WWBs has also become increasingly evident (Lian et al., 2018). As a result, TCs intensify El Niño far more than previously anticipated. Over the past 40 years, significant increases in WNP ACE have been observed

during moderate or stronger El Niño events. The percentage of N3.4 variability explained by WNP ACE has increased at a rate of approximately +11.2 % per decade. In a warming climate, as atmospheric and oceanic energy increases, TCs are expected to contribute more significantly to El Niño intensity. Even after removing the influence of N3.4, WNP ACE shows a steady growth trend. This suggests that the mutually reinforcing relationship between J-A-S ACE and O-N-D N3.4 has become more robust.

TCs modulate ENSO intensity through both oceanic and atmospheric bridges, with their importance in both mechanisms increasing over time. WNP TCs are associated with enhanced wind and circulation anomalies, particularly stronger equatorial westerly winds. These winds exert greater stress near the equator, effectively strengthening or triggering eastward-propagating Kelvin waves. Similarly, TCs have an increasing influence on potential temperature and thermocline depth evolution, contributing to El Niño dynamics through thermocline feedback and zonal advection feedback. Analyses of El Niño events over the past 40 years reveal a closer relationship between TC activity and Kelvin waves. The amplitude of Kelvin waves generated by TCs has increased, a finding further supported by composite analyses of two periods. In addition, intraseasonal variability plays a negligible role in the interaction between TCs and ENSO.

In this study, WNP ACE acts as a bridge between synoptic-scale and interannual-scale systems, quantifying the cumulative contribution of TCs. We propose incorporating the influence of TCs into ENSO forecasting systems. Further investigation is needed to determine whether the intensified impact of TCs over the past 40 years is driven by global warming or decadal variability. Although this study focused on the impact of TCs during El Niño events, the role of WNP ACE during La Niña phases, where it is significantly suppressed, warrants further exploration. Reanalysis datasets have inherent limitations in accurately capturing the intensity and wind structure of TCs. Notably, these datasets tend to underestimate TC wind speeds, a shortcoming that cannot be overlooked. In reality, the westerly winds generated by TCs near the equator are likely stronger than represented, and their significant contribution to El Niño intensity needs to be given greater attention.

Open research

The TCs best-track dataset and ACE calculated in this study are publicly available from the International Best Track Archive for Climate Stewardship (IBTrACS) (https://www.ncei.noaa.gov/products/international-best-track-archive). The monthly ONI index is available from NOAA (https://origin.cpc.ncep.noaa.gov/products/analysis_monitoring/ensostuff/ONI_v5.php). The daily MJO and BSISO index are available from IPRC (https://iprc.soest.hawaii.edu/users/kazuyosh/Bimodal_ISO.html). The monthly SST data with resolution of 2° × 2° from 1981 to 2023 are collected from the Extended Reconstructed Sea Surface Temperature (ERSST) V5 dataset (https://psl.noaa.gov/data/gridded/data.noaa.ersst.v5.html). The hourly wind fields on pressure levels with resolution of 0.25° × 0.25° from 1981 to 2023 are used from ECMWF Reanalysis v5 (ERA5) (https://cds.climate.copernicus.eu/datasets/reanalysis-era5-pressure-levels?tab=download), the National Centers for Environmental Prediction-National Center for Atmospheric Research (NCEP-NCAR) and the Department of Energy (NCEP-DOE) reanalysis dataset. (https://psl.noaa.gov/data/gridded/data.ncep.reanalysis.html and https://psl.noaa.gov/data/gridded/data.ncep.reanalysis2.html). And 5-day potential temperature and current at various depths with resolution of 0.5° × 0.5° from 1981 to 2023 are used by the Simple Ocean Data Assimilation (SODA 3.15.2) (https://dsrs.atmos.umd.edu/DATA/soda3.15.2/REGRIDED/ocean/).

CRediT authorship contribution statement

Xingfang Huang: Writing – original draft, Visualization, Formal analysis. **Fei Huang:** Supervision. **Hengxin Qu:** Methodology. **Tingting Fan:** Writing – review & editing. **Shibin Xu:** Writing – review & editing, Supervision, Funding acquisition, Conceptualization.

Declaration of competing interest

The authors declare that they have no known competing financial interests or personal relationships that could have appeared to influence the work reported in this paper.

Acknowledgement

This work is supported by NSFC (No. 41975061) and Shandong Natural Science Foundation Project (ZR2019ZD12).

Appendix A. Supplementary data

Supplementary data to this article can be found online at https://doi.org/10.1016/j.atmosres.2024.107907.

Data availability

I have shared the link of data in the manuscript.

References

Bell, G.D., Halpert, M.S., Schnell, R.C., Higgins, R.W., Lawrimore, J., Kousky, V.E., Artusa, A., 2000. Climate Assessment for 1999. Bull. Am. Meteorol. Soc. 81 (6), S1–S50. https://doi.org/10.1175/1520-0477(2000)81[s1:CAF]2.0.CO;2.

Bjerknes, J., 1969. Atmospheric teleconnections from the equatorial Pacific. Mon. Weather Rev. 97 (3), 163–172. https://doi.org/10.1175/1520-0493(1969)097<0163:ATFTEP>2.3.CO;2.

Cai, W., Borlace, S., Lengaigne, M., van Rensch, P., Collins, M., Vecchi, G., Jin, F.-F., 2014. Increasing frequency of extreme El Niño events due to greenhouse warming. Nat. Clim. Chang. 4 (2), 111–116. https://doi.org/10.1038/nclimate2100.

Camargo, S.J., Sobel, A.H., 2005. Western north pacific tropical cyclone intensity and ENSO. J. Clim. 18 (15), 2996–3006. https://doi.org/10.1175/JCLI3457.1.

Chia, H.H., Ropelewski, C.F., 2002. The interannual variability in the genesis location of tropical cyclones in the Northwest Pacific. J. Clim. 15 (20), 2934–2944. https://doi.org/10.1175/1520-0442(2002)015<2934:TIVITG>2.0.CO;2.

Elsner, J.B., 2020. Continued increases in the intensity of strong tropical cyclones. Bull. Am. Meteorol. Soc. 101 (8), E1301–E1303. https://doi.org/10.1175/BAMS-D-19-0338.1.

Fedorov, A.V., 2002. The response of the coupled tropical ocean–atmosphere to westerly wind bursts. Q. J. R. Meteorol. Soc. 128 (579), 1–23. https://doi.org/10.1002/qj.200212857901.

Fedorov, A.V., Brierley, C.M., Emanuel, K., 2010. Tropical cyclones and permanent El Niño in the early Pliocene epoch. Nature 463 (7284), 1066–1070. https://doi.org/10.1038/nature08831.

Fedorov, A.V., Hu, S., Lengaigne, M., Guilyardi, E., 2015. The impact of westerly wind bursts and ocean initial state on the development, and diversity of El Niño events. Clim. Dyn. 44 (5–6), 1381–1401. https://doi.org/10.1007/s00382-014-2126-4.

Gan, R., Liu, Q., Huang, G., Hu, K., Li, X., 2023. Greenhouse warming and internal variability increase extreme and Central Pacific El Niño frequency since 1980. Nat. Commun. 14 (1), 394. https://doi.org/10.1038/s41467-023-36053-7.

Harrison, D.E., Giese, B.S., 1991. Episodes of surface westerly winds as observed from islands in the western tropical Pacific. J. Geophys. Res. Oceans 96, 3221–3237. https://doi.org/10.1029/90JC01775.

Hart, R.E., Maue, R.N., Watson, M.C., 2007. Estimating local memory of tropical cyclones through MPI anomaly evolution. Mon. Weather Rev. 135 (12), 3990–4005. https://doi.org/10.1175/2007MWR2038.1.

Hersbach, H., Bell, B., Berrisford, P., Hirahara, S., Horanyi, A., Munoz-Sabater, J., Thepaut, J.-N., 2020. The ERA5 global reanalysis. Q. J. R. Meteorol. Soc. 146 (730), 1999–2049. https://doi.org/10.1002/qj.3803.

Jin, F.F., 1996. Tropical Ocean-atmosphere interaction, the Pacific cold tongue, and the El Niño Southern Oscillation. Science 274 (5284), 76–78. https://doi.org/10.1126/science.274.5284.76.

Jin, F.F., 1997. An equatorial ocean recharge paradigm for ENSO .1. Conceptual model. J. Atmos. Sci. 54 (7), 811–829. https://doi.org/10.1175/1520-0469(1997)054<0811:AEORPF>2.0.CO;2.

Jin, F.F., An, S.I., 1999. Thermocline and zonal advective feedbacks within the equatorial ocean recharge oscillator model for ENSO. Geophys. Res. Lett. 26 (19), 2989–2992. https://doi.org/10.1029/1999GL002297.

Jin, F.F., An, S.I., Timmermann, A., Zhao, J.X., 2003. Strong El Niño events and nonlinear dynamical heating. Geophys. Res. Lett. 30 (3). https://doi.org/10.1029/2002GL016356.

Kalnay, E., Kanamitsu, M., Kistler, R., Collins, W., Deaven, D., Gandin, L., Joseph, D., 1996. The NCEP/NCAR 40-year reanalysis project. Bull. Am. Meteorol. Soc. 77 (3), 437–472. https://doi.org/10.1175/1520-0477(1996)077<0437:TNYRP>2.0.CO;2.

Kanamitsu, M., Ebisuzaki, W., Woollen, J., Yang, S.-K., Hnilo, J.J., Fiorino, M., Potter, G. L., 2002. NCEP–DOE AMIP-II reanalysis (R-2). Bull. Am. Meteorol. Soc. 83 (11), 1631–1644. https://doi.org/10.1175/BAMS-83-11-1631.

Kang, N.-Y., Elsner, J.B., 2015. Trade-off between intensity and frequency of global tropical cyclones. Nat. Clim. Chang. 5 (7). https://doi.org/10.1038/nclimate2646, 661-+.

Kang, N.-Y., Elsner, J.B., 2016. Climate mechanism for stronger Typhoons in a warmer world. J. Clim. 29 (3), 1051–1057. https://doi.org/10.1175/JCLI-D-15-0585.1.

Knapp, K.R., Kruk, M.C., Levinson, D.H., Diamond, H.J., Neumann, C.J., 2010. The international best track archive for climate stewardship (IBTrACS): unifying tropical cyclone data. Bull. Am. Meteorol. Soc. 91 (3), 363–376. https://doi.org/10.1175/2009BAMS2755.1.

Li, H., Hu, A.X., Meehl, G.A., 2023. Role of tropical cyclones in determining ENSO characteristics. Geophys. Res. Lett. 50 (6). https://doi.org/10.1029/2022GL101814.

Lian, T., Chen, D., Tang, Y., Liu, X., Feng, J., Zhou, L., 2018. Linkage between westerly wind bursts and tropical cyclones. Geophys. Res. Lett. 45 (20), 11431–11438. https://doi.org/10.1029/2018GL079745.

Lian, T., Ying, J., Ren, H.-L., Zhang, C., Liu, T., Tan, X.-X., 2019. Effects of tropical cyclones on ENSO. J. Clim. 32 (19), 6423–6443. https://doi.org/10.1175/JCLI-D-18-0821.1.

Liang, Y., Fedorov, A.V., 2021. Linking the Madden-Julian Oscillation, tropical cyclones and westerly wind bursts as part of El Niño development. Clim. Dyn. 57 (3–4), 1039–1060. https://doi.org/10.1007/s00382-021-05757-1.

Lopez, H., Kirtman, B.P., 2014. WWBs, ENSO predictability, the spring barrier and extreme events. J. Geophys. Res. Atmos. 119 (17). https://doi.org/10.1002/2014JD021908.

McPhaden, M.J., Yu, X., 1999. Equatorial waves and the 1997–98 El Niño. Geophys. Res. Lett. 26 (19), 2961–2964. https://doi.org/10.1029/1999GL004901.

Sriver, R.L., Huber, M., Chafik, L., 2013. Excitation of equatorial Kelvin and Yanai waves by tropical cyclones in an ocean general circulation model. Earth Syst. Dynam. 4 (1), 1–10. https://doi.org/10.5194/esd-4-1-2013.

Wang, B., Chan, J.C.L., 2002. How strong ENSO events affect tropical storm activity over the western north pacific. J. Clim. 15 (13), 1643–1658. https://doi.org/10.1175/1520-0442(2002)015<1643:HSEEAT>2.0.CO;2.

Wang, Q., Li, J., 2022a. Feedback of tropical cyclones on El Niño diversity. Part I: phenomenon. Clim. Dyn. 59 (1–2), 169–184. https://doi.org/10.1007/s00382-021-06122-y.

Wang, Q., Li, J., 2022b. Feedback of tropical cyclones on El Niño diversity. Part II: possible mechanism and prediction. Clim. Dyn. 59 (3–4), 715–735. https://doi.org/10.1007/s00382-022-06150-2.

Wang, Q., Tan, Z.-M., 2023. Impact of tropical cyclones over the eastern North Pacific on El Niño-Southern Oscillation intensity. Clim. Dyn. 61, 3103–3126. https://doi.org/10.1007/s00382-023-06723-9.

Wang, C.Z., Li, C.X., Mu, M., Duan, W.S., 2013. Seasonal modulations of different impacts of two types of ENSO events on tropical cyclone activity in the western North Pacific. Clim. Dyn. 40 (11−12), 2887–2902. https://doi.org/10.1007/s00382-012-1434-9.

Wang, Q., Li, J., Jin, F.F., Chan, J.C.L., Wang, C., Ding, R., Xu, Y., 2019. Tropical cyclones act to intensify El Niño. Nat. Commun. 10 (1), 3793. https://doi.org/10.1038/s41467-019-11720-w.

Yamaguchi, M., Chan, J.C.L., Moon, I.J., Yoshida, K., Mizuta, R., 2020. Global warming changes tropical cyclone translation speed. Nat. Commun. 11 (1), 47. https://doi.org/10.1038/s41467-019-13902-y.

Yang, S.-H., Kang, N.-Y., Elsner, J.B., Chun, Y., 2018. Influence of global warming on western north pacific tropical cyclone intensities during 2015. J. Clim. 31 (2), 919–925. https://doi.org/10.1175/JCLI-D-17-0143.1.

Yeh, S.-W., Kug, J.-S., Dewitte, B., Kwon, M.-H., Kirtman, B.P., Jin, F.-F., 2009. El Niño in a changing climate. Nature 461 (7263), 511–514. https://doi.org/10.1038/nature08316.